Bioorganic & Medicinal Chemistry Letters 25 (2015) 5743–5747

Contents lists available at ScienceDirect

Bioorganic & Medicinal Chemistry Letters

journal homepage: www.elsevier.com/locate/bmcl

Discovery of AZ0108, an orally bioavailable phthalazinone PARP inhibitor that blocks centrosome clustering

Jeffrey W. Johannes [a,*], Lynsie Almeida [a], Kevin Daly [a], Andrew D. Ferguson [a], Shaun E. Grosskurth [a], Huiping Guan [a], Tina Howard [b], Stephanos Ioannidis [a], Steven Kazmirski [a], Michelle L. Lamb [a], Nicholas A. Larsen [a], Paul D. Lyne [a], Keith Mikule [a], Claude Ogoe [a], Bo Peng [a], Philip Petteruti [a], Jon A. Read [c], Nancy Su [a], Mark Sylvester [a], Scott Throner [a], Wenxian Wang [a], Xin Wang [a], Jiaquan Wu [a], Qing Ye [a], Yan Yu [a], Xiaolan Zheng [a], David A. Scott [a]

[a] AstraZeneca R&D Boston, 35 Gatehouse Drive, Waltham, MA 02451, United States
[b] AstraZeneca R&D Alderley Park, Macclesfield, Cheshire SK10 4TG, United Kingdom
[c] AstraZeneca R&D Building 310, Milton Science Park, Cambridge CB4 0WG, United Kingdom

ARTICLE INFO

Article history:
Received 4 September 2015
Revised 23 October 2015
Accepted 26 October 2015
Available online 27 October 2015

Keywords:
Centrosome
PARP
Tankyrase
Oncology
Cell cycle

ABSTRACT

The propensity for cancer cells to accumulate additional centrosomes relative to normal cells could be exploited for therapeutic benefit in oncology. Following literature reports that suggested TNKS1 (tankyrase 1) and PARP16 may be involved with spindle structure and function and may play a role in suppressing multi-polar spindle formation in cells with supernumerary centrosomes, we initiated a phenotypic screen to look for small molecule poly (ADP-ribose) polymerase (PARP) enzyme family inhibitors that could produce a multi-polar spindle phenotype via declustering of centrosomes. Screening of AstraZeneca's collection of phthalazinone PARP inhibitors in HeLa cells using high-content screening techniques identified several compounds that produced a multi-polar spindle phenotype at low nanomolar concentrations. Characterization of these compounds across a broad panel of PARP family enzyme assays indicated that they had activity against several PARP family enzymes, including PARP1, 2, 3, 5a, 5b, and 6. Further optimization of these initial hits for improved declustering potency, solubility, permeability, and oral bioavailability resulted in AZ0108, a PARP1, 2, 6 inhibitor that potently inhibits centrosome clustering and is suitable for in vivo efficacy and tolerability studies.

One strategy for treating cancer focuses on targeting the differences between normal cells and tumor cells.[1] An example of such a difference is the propensity for cancer cells to accumulate extra copies of centrosomes, the cellular machinery that serves as the critical microtubule organizing center during mitosis.[2] During the S phase of mitosis, the mother centrosome is copied to yield a daughter centrosome, and these separate to opposite ends of the cell. Each centrosome then serves as a microtubule organizing center for the mitotic spindle. A normal cell entering mitosis with two centrosomes results in a bipolar spindle, which is a prerequisite for proper segregation of sister chromatids to each daughter cell. However, cancer cells that have accumulated extra centrosomes face a conundrum. If a cell has three or more centrosomes during mitosis, this can result in a multi-polar mitotic spindle, leading to improper segregation of chromosomes, and eventual mitotic catastrophe. To overcome this obstacle, cancer cells with supernumerary centrosomes evolve mechanisms to cluster them into two bundles. These two centrosome clusters allow the cell to form a bipolar mitotic spindle and undergo mitosis with proper fidelity.

This observation has led to the hypothesis that disruption of the clustering process in cancer cells with supernumerary centrosomes could lead to mitotic catastrophe while normal cells that can undergo mitosis independent of centrosome clustering mechanisms would be unaffected.[3,4] Discovery of small molecules that could achieve this goal could lead to treatments for cancer. This promise prompted detailed investigations of centrosome clustering to uncover the exact biochemical mechanisms and protein components that are involved in this process. Based on a siRNA screen against all PARP enzymes, TNKS1 (PARP5a) was shown to

Abbreviations: CL, clearance; ent, enantiomer; F%, bioavailability; calc., calculated; enz, enzyme; S2, Schneider 2; PK, pharmacokinetics; PPB, plasma protein binding; PARP, poly (ADP-ribose) polymerase.

* Corresponding author.

http://dx.doi.org/10.1016/j.bmcl.2015.10.079
0960-894X/

be required for the formation of bipolar spindles.[5] Moreover, Kwon et al. performed a genome wide siRNA knockdown screen in Drosophila to uncover which genes may be involved in the centrosome clustering process.[6] Upon treatment with siRNAs to induce a multipolar spindle phenotype in Drosophila S2 cells, they identified genes homologous to the human PARP genes TNKS1 and PARP16. The demonstrated druggability of the PARP enzyme family[7,8] along with AstraZeneca's experience with the PARP inhibitor olaparib prompted us to explore the possibility that a small molecule inhibitor of the PARPs could induce a multi-polar spindle phenotype and prevent the proliferation of cancer cells.

Our initial efforts concentrated on the development of a high content phenotypic assay to screen for small molecules that block centrosome clustering and cause a multi-polar spindle phenotype. This cell-based centrosome declustering assay begins with treatment of HeLa cells with increasing concentrations of compound. After 24 h, the cells are fixed and then the mitotic cells are identified by treatment with a cyclin B antibody. Next, the cells are treated with an antibody towards pericentrin to label the centrosomes. After that, an automated process generates an overlay of the two images and analyzes it to calculate the number of centrosomes observed in each mitotic cell. Mitotic cells with greater than four centrosomes[9] are then assumed to have a multi-polar spindle phenotype. Finally, a declustering EC_{50} is calculated from a dose-response curve generated from a plot of the percentage of mitotic cells with a multi-polar spindle phenotype at eight concentrations ranging from 3 nM to 10 μM. The throughput of this assay allowed for the screening of several hundred compounds at a single concentration, followed up by screening of dozens of compounds with a full centrosome declustering EC_{50}. Experimental details of this assay, including images of the multipolar spindle phenotype, can be found in the Supporting Information.

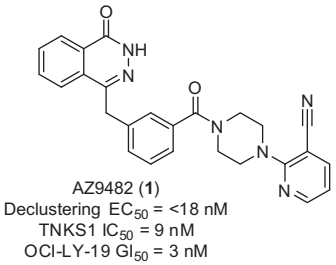

Figure 1. Initial declustering hit from a cell-based screen of PARP inhibitors.

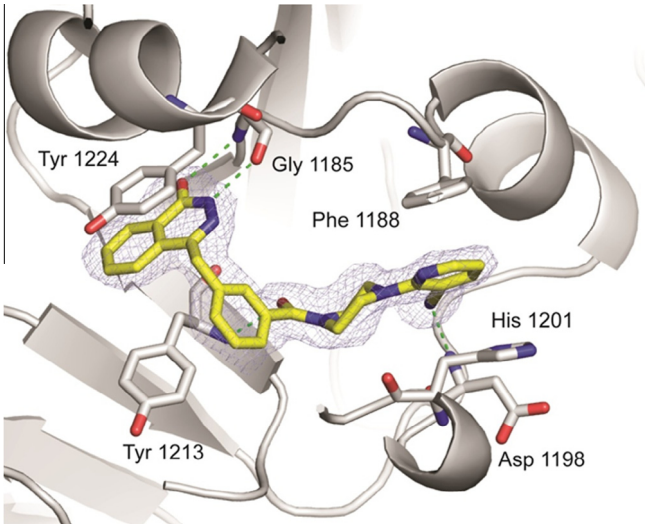

Figure 2. Crystal structure of AZ9482 (compound **1**, yellow) bound to TNKS1 (PDB ID: 5ECE). The $2F_o - F_c$ electron density is displayed at 1σ.

We screened a sub-set of compounds from the AstraZeneca collection containing mostly phthalazinone and quinazolinone based NAD+ mimetic cores. The most potent compound in our initial screen was AZ9482, a phthalazinone PARP inhibitor featuring an amide linkage to a 2-piperazinyl-3-cyano-pyridine (Fig. 1). AZ9482 exhibits very potent centrosome declustering activity in HeLa cells (EC_{50} < 18 nM). Encouragingly, AZ9482 also showed a 3 nM GI_{50} in the DLBCL cell line OCI-LY-19 in a 3-day AlamarBlue assay. Consistent with published siRNA knockdown experiments, AZ9482 was a 9 nM enzyme inhibitor of tankyrase 1 (TNKS1).

This interesting biological profile prompted us to generate a crystal structure of AZ9482 bound to TNKS1 to inform the further optimization of the compound. We used TNKS1 protein as a PARP enzyme for crystallography since the tankyrases have proven to be

Table 1
Fused 1,2,4-triazole improves solubility and intrinsic metabolic stability, while methyl substitution on the piperazine rescues cell potency and further improves intrinsic metabolism

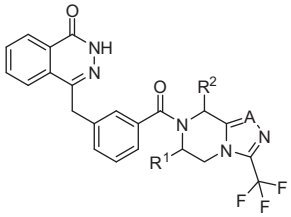

Compd	AZ9482 (**1**)	**2a**	**2b**	**3a**	**3b**	**3c**	**3d**
A	—	N	CH	N	N	N	N
R^1	—	H	H	CH_3 (*S*)	CH_3 (*R*)	H	H
R^2	—	H	H	H	H	CH_3 (*S*)	CH_3 (*R*)
Declustering EC_{50} (μM)	<0.018	0.051	>11	<0.015	>11	5.04	>11
Aq sol. pH 7.4 (μM)	11	984	511	>1000	>1000	612	612
*C*log*P*	1.53	0.79	1.83	1.31	1.31	1.31	1.31
Log*D* 7.4	2.42	1.03	1.66	1.19	1.21		
Hu PPB (% free)	3.2	27	14	19	19		
Rat heps (μL/min 10^6)	134	11	66	<2.2	11		
Rat IV CL (mL/min kg)	83	159		97			
Rat oral bioavailability (%)	12						

a robust PARP enzyme for expression and crystallization.[10,11] The crystal structure of AZ9482 bound to TNKS1 is presented in Figure 2. Similar to other PARP inhibitors,[12,13] the phthalazinone core mimics nicotinamide and binds in the same pocket as the nicotinamide portion of the PARP enzyme cofactor NAD^+. The carbonyl and NH of the phthalazinone form hydrogen bonds with the backbone of Gly1185. The cyano-pyridine moiety serves as an adenine mimetic and binds between the two aromatic residues His1201 and Phe1188. The nitrogen of the nitrile forms a hydrogen bond with the backbone NH of Asp1198. Linking these two parts together is a phenyl amide that interacts with the backbone NH of Tyr1213 via the amide carbonyl.

Intrigued by this compound's ability to induce a multi-polar spindle phenotype and inhibit the growth of cancer cells at low nanomolar concentrations, we were eager to test the consequences of this mechanism of action in vivo in a suitable xenograft model. However, as outlined in Table 1, compound **1** has poor aqueous solubility (11 μM) and DMPK properties. When subjected to human microsomal (hu mics) or rat hepatocyte (rat heps) incubations (see Supporting Information Table S1), compound **1** is rapidly metabolized resulting in very high intrinsic clearances (CL_{int}). This high intrinsic hepatic clearance is also reflected in vivo, where the rat clearance (CL) following IV bolus was measured at 83 mL/min kg. Moreover, the low solubility likely resulted in poor fraction absorbed and high plasma clearance led to low bioavailability (12%) following oral dosing in rat. With this data in hand, we focused our medicinal chemistry efforts on improving the properties of our analogs with an ultimate goal to increase water solubility. Our designs also concentrated on mitigating the in vivo clearance liability of the series while maintaining potency in the centrosome declustering assay.

The amide linkage in compound **1** served as a handle for rapid generation of analogs, wherein a large number of diverse piperazines were incorporated. From this set, we uncovered compound **2a**, a compound featuring a fused triazolopiperazine moiety which showed greatly improved physicochemical properties compared to initial hit **1** (Table 1). Compound **2a** was 51 nM in the declustering assay and also had an aqueous solubility of 984 μM. More importantly, **2a** had greatly reduced lipophilicity (calculated reduction in *C*log*P*) and correspondingly low CL_{int} in rat heps. Unexpectedly, this compound did not show a corresponding improvement in rat CL in vivo; its measured rat clearance was very high at 159 (mL/min kg). Interestingly, close analog **2b**, which has swapped nitrogen for carbon to create a fused imidazopiperazine, was not potent in our declustering assay. We surmised that this nitrogen in compound **2a** serves as a hydrogen bond acceptor for the backbone NH of Asp1198, taking the place of the nitrile moiety in **1**.

Having identified compound **2a**, which featured improved CL_{int} and solubility, we sought to fix the poor in vivo clearance of this series. Guided by the observation of oxidative metabolism of **2a** at the methylene groups alpha to the amide nitrogen in vivo, we explored methyl group substitution at these positions (Table 1). Methyl substitution at the pseudo-benzylic methylene between the piperazine nitrogen and the triazole was not tolerated; compounds **3c** and **3d** lost cell potency significantly. Surprisingly, addition of a methyl group at the opposite methylene alpha to the amide nitrogen was tolerated, provided the compound had (*S*) stereochemistry. (*S*)-methyl compound **3a** had improved declustering potency comparable to **1**, while (*R*)-methyl compound **3b** had an EC_{50} of >11 μM in the declustering assay. Moreover, compound **3a** was in a much better physicochemical property space and DMPK space. Compound **3a** had a measured aqueous solubility of >1000 μM compared to **1**, which had a solubility of only 11 μM. Most importantly, (*S*)-methyl compound **3a** was more stable in rat hepatocytes compared to **2a**, with an intrinsic clearance of <2.2 μL/min 10^6 cells. In spite of this, the in vivo PK of compound **3a** still showed poor clearance in rat (CL = 97 mL/min kg).

Table 2
Difluoro substitution on the benzylic linker improves rat CL

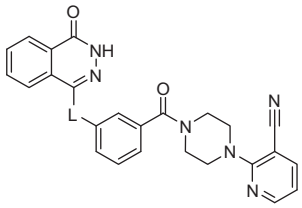

Compd*	L	Declustering EC_{50} (μM)	Rat heps (μL/min 10^6)	Rat CL (mL/min kg)	Caco2 AB P_{app} (10^{-6} cm/s)
1	CH_2	<0.018	134	83	13
4	O	9.18	39	21	12
5	NH	9.33	31		
6	S	0.311	208	97	
7	CF_2	0.573	109	25	5†
8	$CHCH_3$	0.027	109	122	
9	CHOH	0.115	43	86	
10	CHF	0.140	192		
11	$CHNH_2$	0.057	39	30	0.2

* Data for most cell potent, chirally pure enantiomer where applicable.
† 39% mass recovery.

Other metabolites produced in vivo in rat from **2a** included hydroxylation of the benzylic methylene linker between the phthalazinone core and the phenyl ring. Following this observation, we designed and synthesized a series of compounds featuring alterations and substituents at the benzylic methylene linker (Table 2, position L in the structure). We chose to make these alterations to **1**, since many of the substituents would create a stereogenic center at position L and the 3-cyano-2-piperazinyl-pyridine moiety was commercially available, simplifying the synthesis and chiral purification of these compounds. Changing the CH_2 linker to O or NH caused a large reduction in declustering potency. Nevertheless, compounds **4** and **5** had improved rat heps, and for compound **4**, this manifested itself in a greatly improved rat in vivo clearance of 21 mL/min kg, an almost 4-fold improvement over **1**. Encouraged by this, we prepared additional analogs such as sulfur linked compound **6**, which retained some declustering cell potency but showed no improvement rat hepatocytes or in vivo clearance. Interestingly, CF_2 linked compound **7** had greatly improved in vivo clearance and still retained some declustering cell potency.[14] We also explored compounds that kept the carbon linker while introducing a substituent such as CH_3, OH, F, and NH_2 (compounds **8**–**11**). In these cases, only one enantiomer was appreciably active in the declustering cell assay. Of this set, only compound **11** retained cell potency while showing an improvement in both in vitro and in vivo PK. Examining **7** versus **11** with the goal of optimizing this series to an orally bioavailable compound, we chose to progress with compound **7**, since it retained permeability while compound **11** had very low permeability in a Caco2 permeability assay.[15,16]

Combining the difluoro linker with the (*S*)-methyl fused triazolopiperazine adenine mimetic led to compound **14a** (Table 3) which had improved cell potency (216 nM) relative to compound **7**. More importantly, this compound had a clearance of 33 mL/min kg with an oral bioavailability of 43%, demonstrating that the beneficial effects of the CF_2 linker on PK carried over to the more potent fused triazolopiperazine sub-series. Compound **14a** also had favorable solubility, and its overall potency, property and PK profile served as the basis for the final phase of optimization.

Table 3
Modification of the 1,2,4-triazole 3-substituent improves bioavailability leading to AZ0108 (compound **14f**)

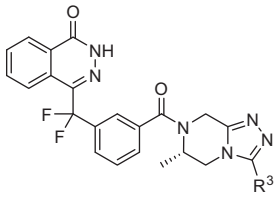

Compd	R^3	R^3 Hammett σ_p	Decl. EC_{50} (μM)	Aq sol. pH 7.4 (μM)	Log*D* 7.4	Rat CL[†]	Rat oral F%	Caco2 AB P_{app}[‡]	Caco2 efflux ratio
14a	CF_3	0.54	0.216	268	2.3	33	43	9.3	3.6
14b	iPr	−0.15	0.102	>928	2.1	23	3	4.0	13.5
14c	cyBu	−0.14	0.049	619	2.4	36	5	4.8	11.0
14d	tBu	−0.20	0.087	473	2.5	60	15	6.2	5.5
14e	$C(Me)_2F$	−0.01[*]	0.043	436	2.4	38	57	8.4	4.2
14f (AZ0108)	$C(Me)F_2$	0.21[*]	0.053	238	2.7	17	79	18.5	2.3

[*] Calculated using ACD labs.
[†] Unit: mL/min kg.
[‡] Unit: 10^{-6} cm/s.

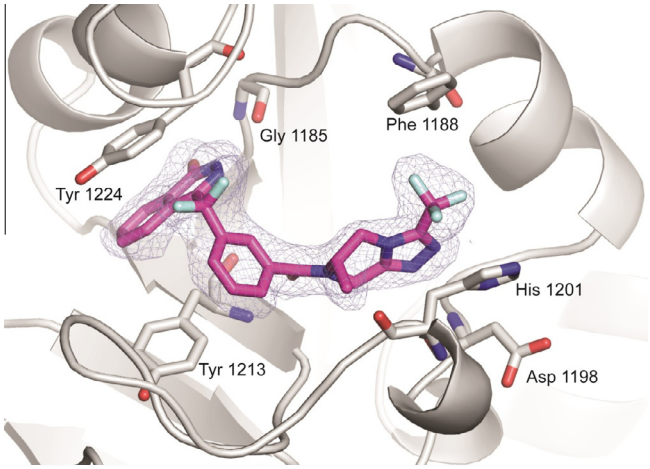

Figure 3. Crystal structure of compound **14a** (magenta) bound to TNKS1 (PDB ID: 5EBT). The $2F_o - F_c$ electron density is displayed at 1σ.

We next obtained a crystal structure of **14a** bound to TNKS1 (Fig. 3). As expected, the phthalazinone core of compound **14a** binds in a similar manner as **1**. The switch to a CF_2 linker causes a slight increase in the dihedral angle between the phthalazinone core and the linker-phenyl bond (−93° for the CF_2 linker in compound **14a** vs −83° for the CH_2 linker in **1**). The amide linkage engages Tyr1213 just as compound **1** does. The structure shows that the (*S*)-methyl of the piperazine fits into a small hydrophobic pocket near the D-loop. The 1,2,4-triazole moiety forms a hydrogen bond to the backbone NH of Asp1198 mimicking the nitrile of AZ9482 as we had hypothesized. The trifluoromethyl group lies in the hydrophobic cleft between aromatic residues His1202 and Phe1188 in the adenine pocket. Both compounds **1** and **14a** mimic the NAD+ cofactor very closely, and based on this, we hypothesize that these compounds would have a similar binding mode in other PARPs.

Table 4
PARP family enzyme and cell data for and AZ9482 (**1**), AZ0108 (**14f**) and olaparib

	AZ9482 (**1**)	AZ0108 (**14f**)	Olaparib
PARP1 Enz IC_{50} (μM)	0.001	<0.03	0.001
PARP2 Enz IC_{50} (μM)	0.001	<0.03	0.003
PARP3 Enz IC_{50} (μM)	0.046	2.8	0.046
TNKS1 Enz IC_{50} (μM)	0.009	3.2	1.9
TNKS2 Enz IC_{50} (μM)	0.16	>3	1.7
PARP6 Enz IC_{50} (μM)	0.64	0.083	1.8
Declustering EC_{50} (μM)	<0.018	0.053	>11
DLD-1 Wnt IC_{50} (μM)	0.222	>3	>3
OCI-LY-19 GI_{50} (μM)	0.003	0.017	0.849

In considering the further optimization of **14a**, we hypothesized that modulation of the electronic nature of the substituent at R^3 (Table 3) would influence the strength of the backbone hydrogen bond between the triazole and Asp1198. We also strove to keep the R^3 group hydrophobic, consistent with the structure-activity relationships we had observed. To test this hypothesis, a series of compounds (**14b–d** in Table 3) were made featuring a lipophilic, electron donating group at R^3 as approximated by Hammett σ_p values.[17] Introduction of donating lipophilic groups such as isopropyl, cyclobutyl, or *t*-butyl (compounds **14b–d**) improved declustering cell potency as desired, but they also exhibited a sharp drop in oral bioavailability in rat. Bioavailability appeared to drop after crossing a threshold Caco2 efflux ratio of approximately 10. For example, iPr analog **14b** had only 3% oral bioavailability, with a Caco2 efflux ratio of 13.5. The most potent compound in this set was the cyclobutyl analog **14c**, which was 49 nM in the declustering assay, but it had only 5% bioavailability and a Caco2 efflux ratio 11.0.

Clearly, alkyl groups at R^3 gave the improvement in potency that we sought, but at the expense of higher efflux ratios and poor bioavailability. We suspected that higher efflux arose from a more electron rich triazole due to the strongly electron donating character of these alkyl groups (negative Hammett σ_p values). A similar trend in the bioavailability of alkyl versus trifluoromethyl triazoles was observed during the optimization of sitagliptin.[18,19] In order to tune the electronics of the group at R^3, addition of a single fluorine atom to **14b** gave rise to fluoro-isopropyl analog **14e**, which has a near electron-neutral predicted Hammett σ_p value. Gratifyingly, introduction of this fluorine atom led to a 5-fold improvement in declustering potency compared to **14a** while maintaining good rat pharmacokinetics. The difluoroethyl analog **14f** (AZ0108), which has a predicted σ_p value that falls between the highly withdrawing trifluoromethyl and the electro-neutral fluoroisopropyl, showed the best balance of potency and pharmacokinetics. In addition to excellent declustering potency and low in vivo rat Cl, **14f** had good solubility and the highest permeability of all the analogs tested, with correspondingly good oral bioavailability.

Overall, **14f** shows several notable improvements compared to **1**. Both compounds inhibit centrosome clustering at in HeLa cells

at <100 nM, and show a very potent GI_{50} against OCI-LY-19 cells. In spite of having higher log*D*, **14f** is more soluble than compound **1** and has much better human in vitro pharmacokinetic properties. Across mouse, rat and dog, **14f** has an excellent in vivo pharmacokinetic profile. (See the Supporting Information Table S1 for further details on the DMPK of compounds **1** and **14f**).

AZ9482 (**1**) and AZ0108 (**14f**) have different inhibition profiles of the PARP enzyme family as shown in Table 4. Compound **1** is a multi-PARP enzyme inhibitor, with significant inhibition of PARPs 1, 2, 3 and TNKS1/2 as well as PARP6 (a mono(ADP-ribosyl) transferase).[20] Compound **1** was also active in a Wnt pathway reporter assay, producing a DLD-1 firefly luciferase IC_{50} of 222 nM, presumably due to the TNKS1/2 activity.[21] In contrast to **1**, compound **14f** is more selective in its enzyme inhibition profile and effects on cellular pathways and phenotypes. Specifically, **14f** inhibits PARPs 1, 2, and 6 with approximately 100-fold selectivity against PARP3 and TNKS1. Consistent with this lack of potency towards tankyrase, **14f** is not active in a DLD-1 Wnt luciferase reporter assay. In contrast, olaparib[22] is a very potent PARP1 inhibitor, which also carries some PARP2 and PARP3 activity, but is selective against the tankyrases and PARP6. Olaparib has an IC_{50} of >3 μM in the DLD-1 Wnt luciferase reporter assay as expected, but also shows little effect in the declustering assay. These data suggest that PARP6 enzyme inhibition may contribute to a declustering phenotype in HeLa cells. Additionally, the data imply that small molecule inhibition of the PARP catalytic domain of the tankyrases does not contribute to this phenotype. However, since these compounds are not perfectly selective for PARP6, it cannot be ruled out that inhibition of the PARP catalytic domain of other PARP family enzymes also contributes to the phenotype. In depth details of the biological effects of PARP6 enzyme inhibition both in vitro and in vivo by AZ9482 (**1**) and AZ0108 (**14f**) will be reported in a separate publication.[23]

In conclusion, using a cell-based phenotypic screen for compounds that can inhibit centrosome clustering in cancer cells, we screened a subset of the AstraZeneca collection containing known PARP inhibitor scaffolds. This screen identified AZ9482 (**1**) as a potent inhibitor of centrosome clustering. In order to test the effects of centrosome declustering in vivo, we optimized **1** using structure and property guided medicinal chemistry design to produce AZ0108 (**14f**), an orally bioavailable, PARP1,2,6 inhibitor that causes a multi-polar spindle phenotype at double digit nM concentrations. Important highlights of the optimization include: (1) identification of a triazolopiperazine with improved physicochemical properties, (2) chiral methyl substitution on the piperazine to improve potency, (3) blocking metabolism and improving pharmacokinetics by difluorination of the methylene linker, and (4) tuning the electronics of the triazole moiety to improve potency and oral bioavailability. Both AZ9482 (**1**) and AZ0108 (**14f**) have been utilized as in vitro tools[24] and in vivo probes[25] to investigate the biological consequences of inhibiting centrosome clustering through PARP enzymes. Experimental details on the preparation of AZ9482 and AZ0108 can be found in the Supporting Information.

Supplementary data

Supplementary data associated with this article can be found, in the online version, at http://dx.doi.org/10.1016/j.bmcl.2015.10.079.

References and notes

1. Hanahan, D.; Weinberg, R. A. *Cell* **2011**, *144*, 646.
2. Nigg, E. A. *Nat. Rev. Cancer* **2002**, *2*, 815.
3. Krämer, A.; Maier, B.; Bartek, J. *Mol. Oncol.* **2011**, *5*, 324.
4. Gergely, F.; Basto, R. *Genes Dev.* **2008**, *22*, 2291.
5. Chang, P.; Coughlin, M.; Mitchison, T. J. *Nat. Cell Biol.* **2005**, *7*, 1133.
6. Kwon, M.; Godinho, S. A.; Chandhok, N. S.; Ganem, N. J.; Azioune, A.; Thery, M.; Pellman, D. *Genes Dev.* **2008**, *22*, 2189.
7. Amé, J. C.; Spenlehauer, C.; de Murcia, G. *BioEssays* **2004**, *26*, 882.
8. Rouleau, M.; Patel, A.; Hendzel, M. J.; Kaufmann, S. H.; Poirier, G. G. *Nat. Rev. Cancer* **2010**, *10*, 293.
9. Setting the cut-off at >4 centrosomes gave a bigger assay window compared to using a cut-off of >3 or >2 centrosomes.
10. Lehtiö, L.; Collins, R.; van den Berg, S.; Johansson, A.; Dahlgren, L. G.; Hammarström, M.; Helleday, T.; Holmberg-Schiavone, L.; Karlberg, T.; Weigelt, J. *J. Mol. Biol.* **2008**, *379*, 136.
11. http://www.thesgc.org/structures/2rf5#mandm.
12. Kirby, C. A.; Cheung, A.; Fazal, A.; Shultz, M. D.; Stams, T. *Acta Crystallogr., Sect. F: Struct. Biol. Cryst. Commun.* **2012**, *68*, 115.
13. Narwal, M.; Venkannagari, H.; Lehtiö, L. *J. Med. Chem.* **2012**, *55*, 1360.
14. Purser, S.; Moore, P. R.; Swallow, S.; Gouverneur, V. *Chem. Soc. Rev.* **2008**, *37*, 320.
15. Mandagere, A. K.; Thompson, T. N.; Hwang, K. K. *J. Med. Chem.* **2002**, *45*, 304.
16. Skolnik, S.; Lin, X.; Wang, J.; Chen, X. H.; He, T.; Zhang, B. *J. Pharm. Sci.* **2010**, *99*, 3246.
17. Hansch, C.; Leo, A.; Taft, R. W. *Chem. Rev.* **1991**, *91*, 165.
18. Kim, D.; Wang, L.; Beconi, M.; Eiermann, G. J.; Fisher, M. H.; He, H.; Hickey, G. J.; Kowalchick, J. E.; Leiting, B.; Lyons, K.; Marsilio, F.; McCann, M. E.; Patel, R. A.; Petrov, A.; Scapin, G.; Patel, S. B.; Roy, R. S.; Wu, J. K.; Wyvratt, M. J.; Zhang, B. B.; Zhu, L.; Thornberry, N. A.; Weber, A. E. *J. Med. Chem.* **2005**, *48*, 141.
19. Kim, D.; Kowalchick, J. E.; Edmondson, S. D.; Mastracchio, A.; Xu, J.; Eiermann, G. J.; Leiting, B.; Wu, J. K.; Pryor, K. D.; Patel, R. A.; He, H.; Lyons, K. A.; Thornberry, N. A.; Weber, A. E. *Bioorg. Med. Chem. Lett.* **2007**, *17*, 3373.
20. Tuncel, H.; Tanaka, S.; Oka, S.; Nakai, S.; Fukutomi, R.; Okamoto, M.; Ota, T.; Kaneko, H.; Tatsuka, M.; Shimamoto, F. *Int. J. Oncol.* **2012**, *41*, 2079.
21. Huang, S. M.; Mishina, Y. M.; Liu, S.; Cheung, A.; Stegmeier, F.; Michaud, G. A.; Charlat, O.; Wiellette, E.; Zhang, Y.; Wiessner, S.; Hild, M.; Shi, X.; Wilson, C. J.; Mickanin, C.; Myer, V.; Fazal, A.; Tomlinson, R.; Serluca, F.; Shao, W.; Cheng, H.; Shultz, M.; Rau, C.; Schirle, M.; Schlegl, J.; Ghidelli, S.; Fawell, S.; Lu, C.; Curtis, D.; Kirschner, M. W.; Lengauer, C.; Finan, P. M.; Tallarico, J. A.; Bouwmeester, T.; Porter, J. A.; Bauer, A.; Cong, F. *Nature* **2009**, *461*, 614.
22. Menear, K. A.; Adcock, C.; Boulter, R.; Cockcroft, X. L.; Copsey, L.; Cranston, A.; Dillon, K. J.; Drzewiecki, J.; Garman, S.; Gomez, S.; Javaid, H.; Kerrigan, F.; Knights, C.; Lau, A.; Loh, V. M.; Matthews, I. T.; Moore, S.; O'Connor, M. J.; Smith, G. C.; Martin, N. M. *J. Med. Chem.* **2008**, *51*, 6581.
23. Wang, Z.; Petteruti, P.; Wang, X.; Wang, W.; Gharahdaghi, F.; Wu, J.; Su, N.; Cheung, T.; Mayo, M.; Scott, D.; Johannes, J.; Lamb, M.; Lawson, D.; Collins, M.; Nadella, P.; Reimer, C.; Lyne, P.; Zinda, M.; Mikule, K.; Fawell, S.; Grosskurth, S. Submitted manuscript.
24. Grosskurth, S.; Petteruti, P.; Wang, X.; Mikule, K. *Mol. Cancer Ther.* **2013**, *12*, A134.
25. Mayo, M. F.; Grosskurth, S.; Wang, X.; Petteruti, P.; Nadella, P.; Reimer, C.; Mikule, K. *Mol. Cancer Ther.* **2013**, *12*, A221.